CFD modelling of mass transfer with and without chemical reaction in the liquid-liquid slug flow capillary microreactor

M. N. Kashid [a,b,*], D. W. Agar [a] and S. Turek [b]

[a] *Institute of Reaction Engineering, University of Dortmund, 44227 Dortmund, Germany*

[b] *Institute for Applied Mathematics, University of Dortmund, 44227 Dortmund, Germany*

Abstract

A finite element based computational fluid dynamics (CFD) model was developed to study the flow patterns within the slugs and mass transfer with and without superimposed chemical reaction between two consecutive slugs in the liquid-liquid slug flow capillary microreactor. Since the slug flow is a series of alternate slugs of one phase separated by the other, a single element consisting of a slug of each phase was considered. The two slugs in a single domain were distinguished by two kinematic viscosities. The effects of various operating conditions on circulation patterns, mass transfer and reaction are discussed in detail. Finally, the results are compared with experimental data from the literature.

Key words: Slug flow microreactor, Finite element CFD model, Interphase mass transfer, Chemical reaction

* Corresponding author
Email: kashid@bci.uni-dortmund.de

1 Introduction

Microreactors are an attractive new tool for chemical engineers due to their diverse benefits over the conventional reactors. The liquid-liquid slug flow microreactor can be seen as an alternative to suspended drop reactors for mass transfer limited and strongly exothermic reactions. In this reactor arrangement the phases are present as a series of alternating moving slugs, constituting a series of well-defined individual subvolumes and thus interfacial area which thus fulfils the basic requirement for *a priori* prediction of mass transfer rates. In addition to this, one is able to adjust two independent transport mechanisms: convection due to internal circulations within each slug and interphase diffusion between two consecutive slugs. The high interfacial area in comparison with other contactors also enhances the mass transfer by improving the surface renewal at the interface due internal circulations, which arise because of the shear between slug axis and continuous phase or capillary wall. The possibility of precise temperature profiling along the axial co-ordinate represents the further advantage of this reactor type.

A number of theoretical and numerical models have been developed to describe mass transfer with and without chemical reactions between a drop and continuous phases (for example, Piarah *et. al.*[17]). Since microreactor technology is relatively new area, very few studies have been published on single phase and two phase flow at this scale(for example, [9], [4], [11]). Slug flow has also been studied by many researchers and is referred to as bubble train flow or Taylor bubble flow for gas-liquid flows, while it is called segmented flow, liquid train or slug flow for liquid-liquid flows. Simulations with a simple reaction engineering model for liquid-liquid slug flow were carried out in [3] and it was found that increased flow velocity enhances the mass transfer by inducing more intensive internal circulations within the slugs. Furthermore, a numerical model was developed to describe the internal flow patterns within the fluid segments [5] and the transfer of the dissolved chemical species within and across the segments for liquid-liquid slug flow. The flow was represented by two stagnant, adjacent rectangular units which are linked at both ends to form a continuous loop. The model was validated with various sets of experimental results and showed good prediction of flow field and mass transfer. In one of our previous publications [7], we have characterised internal circulations within the slugs using simplified CFD simulations and visualised with these with the help of PIV experiments and CFD particle tracing. Both visualisation techniques

showed qualitatively reliable circulations corresponding to those reported in the literature for liquid slugs in gas-liquid and liquid-liquid slug flow. Recently, Tanthapanichakoon *et. al.*[13] have carried out 2D and 3D simulations to study mixing behaviour in the liquid slug of liquid-liquid slug flow and proposed a modified Peclet number for calculating mixing in liquid slugs.

Different methods are available to model two immiscible fluids such as level set, volume of fluid, marker particle, lattice boltzmann, front tracking and so on. A short review of these methods can be found in [19]. In one of our previous publications [8], we have developed a free surface model to understand the generation of slug flow. However, to solve the complete system for mass transfer with chemical reaction using these methods requires extensive computational resources. So in the present work, a model has been developed to study the mass transfer with chemical reaction in the liquid-liquid slug flow. Similar type of model has already been developed to study the reaction in the liquid-liquid slug flow by Harries *et al* [5], however, they have used viscosity ratio equal to 1 while the present model is applicable for all viscosity ratios. Also, due to the superior experience of the in-house developed finite element code particularly for single phase flow, the model equations are implemented in open source, finite element software, FEATFLOW which is developed in-house. The objective was to develop a prototype model which can be used for any liquid-liquid system with fixed interface location for mass transfer with and without chemical reaction. The numerical model, its solution and the results obtained are discussed in the following sections. The effects of operating conditions on flow patterns, mass transfer and chemical reaction are presented in detail. Finally, the results were compared with the experimental and numerical results of Harries *et. al.* [5].

2 Numerical Model

2.1 Problem definition

In the present work, unsteady flow behaviour and mass transfer with and without superimposed chemical reaction in slug flow is considered. Since the slug flow is an alternating flow of two immiscible liquid phases, it has two independent flow patterns in a single slug unit: a pair of two consecutive

slugs of different phases. The following assumptions were considered to be reasonable for studying such a problem:

- Both slugs are comprised of Newtonian, viscous and incompressible fluids
- The shape of the slug and volume remains constant
- The flow is laminar and the mass diffusivity is constant in both slugs
- There is no interfacial resistance to mass transfer
- The mass transfer and reaction does not affect the flow patterns within the slugs.

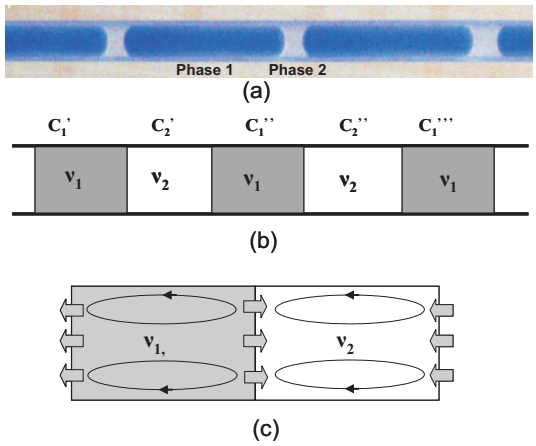

Fig. 1. Liquid-liquid slug flow (a) Experimental snapshot, (b) Schematic representation of the slug flow, and (c) computational domain

An experimental snapshot and the computational domain for this problem is as depicted in Figure 1. The experimental snapshot shows well-defined slug flow consisting of alternate slugs of the two phases. This flow regime with mass transfer of single species can be schematically represented as shown in Figure 1b. Though the experimental snapshot shows that the interface between two slugs is curved, we have considered to be a straight line parallel to y-axis to simplify CFD problem formulation. C_1 and C_2 are the concentrations of any species in phase 1 and 2 having kinematic viscosities of ν_1 and ν_2, respectively. Each slug has different species concentration depending on the residence time of the slug in the capillary microreactor. Since the microreactor comprises of the slugs of lengths ranging from μm to mm, the residence time difference between two consecutive slugs of one phase can be neglected. Therefore, it is considered that c_1' is equal to c_1" which implies that c_2' and c_2" are similar i. e. translational symmetry and the problem is reduced to a single slug unit (the pair of two slugs of two phases as shown in Figure 1c) which can reduce the computational effort significantly. As

shown in figure 1c, the arrows indicate that each slug exchanges mass and momentum with its two neighbours.

2.2 Fluid flow

The computational domain shown in Figure 1c was considered as two dimensional. The velocity u and pressure p for this problem were solved by the following Navier-Stokes equation:

$$\nabla \cdot \mathbf{u} = 0 \tag{1}$$

$$\frac{\partial(\rho \mathbf{u})}{\partial t} + \rho \mathbf{u} \cdot \nabla \mathbf{u} - \nabla \cdot (2\mu S) + \nabla p = f \qquad \Omega \in \mathbb{R}^2 \times [0, \mathrm{T}] \tag{2}$$

where ρ and μ are the density and dynamic viscosity respectively while S is the rate deformation tensor. They are defined as follows:

$$\begin{aligned} \rho &= \rho_0 f(x, y) \\ \mu &= \mu_0 f(x, y) \\ S &= \frac{1}{2}(\nabla \mathbf{u} + \nabla^T \mathbf{u}) \end{aligned} \tag{3}$$

Two densities and viscosities were defined to represent the two phases in the same domain. However, there is an interface between the two slugs where the transport across it is due to diffusion only. This was represented by the concept of moving boundaries and the y-component of the velocity of interface containing cells was set to average slug flow velocity. In addition to this, there is a need to connect the two sides of the domain like a strip of paper wrapped around in a continuous loop. The connection was implemented using the concept of periodic boundary, and interface boundary conditions were applied at this connection which is referred to as the interface. Thus, the interface and periodically connected interface satisfies the following condition for momentum:

$$\mu_1 \frac{\partial u_1}{\partial \mathbf{n}_1} = \mu_2 \frac{\partial u_2}{\partial \mathbf{n}_2} \tag{4}$$

where μ_i, u_i and $\mathbf{n}_i$ are the dynamic viscosities, velocities and unit normal to the interface in the i^{th} domain, respectively. Since the interface is parallel to the y-axis, the above equation can be written as follows:

$$\mu_1 \frac{\partial u_1}{\partial x} = \mu_2 \frac{\partial u_2}{\partial x} \tag{5}$$

The transfer of species within the two phases is governed by the general convection-diffusion equations:

$$\frac{\partial C_{11}}{\partial t} + \mathbf{u}_1 \cdot \nabla C_{11} = D_{11} \Delta C_{11} \tag{6}$$

$$\frac{\partial C_{12}}{\partial t} + \mathbf{u}_2 \cdot \nabla C_{12} = D_{12} \Delta C_{12} \tag{7}$$

where C_{11} and C_{12} are the concentration of species 1 in phase 1 and 2, respectively. The natural boundary conditions were defined at the interface to satisfy the flux continuity at the interface by the following relation:

$$D_{11} \frac{\partial C_{11}}{\partial x} = D_{12} \frac{\partial C_{12}}{\partial x} \tag{8}$$

$$C_{12} = m C_{11} \tag{9}$$

where D_{11} and D_{12} are the diffusivities of species 1 in phase 1 and 2 respectively. In the above formulation, the species will transfer from the higher concentration to lower until equal concentration in both phases is achieved i.e. distribution coefficient (m) equal to 1. However, this is not always true and therefore the discontinuity was treated as given in Yang and Mao [20], who rended the concentration field continuous across the interface by making following transformations:

$$\hat{C_{11}} = C_{11} \sqrt{m} \tag{10}$$

$$\hat{C_{12}} = C_{12} / \sqrt{m} \tag{11}$$

The concentration condition at the interface is:

$$\hat{C_{11}} = \hat{C_{12}} \tag{12}$$

Therefore, at the interface, the diffusion coefficients D_{11} and D_{12} are locally replaced by $D_{11}/\sqrt{m}$ and $D_{12}\sqrt{m}$ to satisfy the original mass flux continuity. The interfacial boundary condition (Equation 8) becomes:

$$D_{11}/\sqrt{m} \frac{\partial \hat{C}_{11}}{\partial x} = D_{12} \sqrt{m} \frac{\partial \hat{C}_{12}}{\partial x} \tag{13}$$

Thus, the final equations for the species transport for two phases can be written as:

$$\frac{\partial \hat{C}_{11}}{\partial(\sqrt{m}t)} + \frac{1}{\sqrt{m}}\mathbf{u} \cdot \nabla \hat{C}_{11} = \frac{1}{\sqrt{m}}\nabla \cdot (D\nabla \hat{C}_{11}) \tag{14}$$

$$\frac{\partial \hat{C}_{12}}{\partial(\frac{1}{\sqrt{m}}t)} + \sqrt{m}\mathbf{u} \cdot \nabla \hat{C}_{12} = \sqrt{m}\nabla \cdot (D\nabla \hat{C}_{12}) \tag{15}$$

In general, the species transport equation takes the form of momentum equation given below:

$$\frac{\partial \hat{C}}{\partial t} + \mathbf{u} \cdot \nabla \hat{C} = \nabla \cdot (\hat{D}\nabla \hat{C}) \tag{16}$$

2.4 Chemical reaction

The chemical reaction in CFD formulation is represented as a source or sink term in the convection-diffusion equation depending on the kinetics of the reaction. So, in general, the convection-diffusion-reaction equation can be written as follows:

$$\frac{\partial C_{ik}}{\partial t} + \mathbf{u} \cdot \nabla C_{ik} = \nabla \cdot (D_{ik}\nabla C_{ik}) \pm r_{ik} \tag{17}$$

Where, C_{ik}, D_{ik} and r_{ik} are the concentration, diffusivity and rate of reaction of i^{th} component in k^{th} phase.

The above equations are the generalised form of the equation 6 and 7 with additional reaction term. When the reaction takes place in just one of the phases, one or more species from non-reactive phase are transferred by diffusion to the reaction phase where the reaction takes place. This reaction creates the concentration gradient across the interface and enhances the rate of species transfer. As with mass transfer, it is physically possible that a entire species or more than the amount of species required for the reaction can pass into the other phase. This problem can be solved by carrying out the transformation discussed in the above mass transfer section which is sometimes referred as partitioning.

The equations are first discretised using first order accurate, implicit Backward Euler(BE) scheme for time, which belongs to the $one - step - \theta - scheme$, while a finite element (FEM) approach was used for spatial discretisation of the governing equations. The details of both discretisations are provided in Turek [15] and Ouazzi [16]. The set of resulting formulations are implemented in the, open source software, FEATFLOW which is developed in-house ($www.featflow.de$).

For all simulations, the slug unit was kept stationary and the walls were moved with the average slug flow velocity and therefore the velocity of interface containing cells was set to zero. A no-slip boundary condition was implemented at the moving walls. The natural boundary conditions at the interface describes the transfer of momentum and species by diffusion across it according to the Equation 5 and 8, respectively . Similar boundary conditions were implemented to the periodically connected interface. For species transport, the Neumann type boundary condition (zero species flux) was implemented to the moving walls as shown in the following:

$$\hat{D}\nabla\hat{C} \cdot \mathbf{n} = 0 \tag{18}$$

For the reaction, the boundary conditions are similar to those used for mass transfer alone but it is important to identify the reactive phase. It varies from system to system and is discussed in detail with an example in the model validation section.

The FEATFLOW package gives the freedom to use two different approaches namely, a coupled approach and a projection approach to treat the discretised nonlinear system. The coupled approach solves for velocity and pressure simultaneously, provides the best stability behaviour, but requires greater numerical efforts, while the projection solver decouples velocity and pressure, reduces the problem to the solution of a sequence of scalar problems [15] and is well-suited for non-stationary configurations. So, in this study, the projected solver was deemed more suitable to simulate the flow field. The equations for mass transfer were solved using the projected solver in a manner similar to the momentum equations. The simulation were carried out in a transient manner i.e. first the steady state velocity and pressure profiles were established and then they were employed into mass transfer calculations.

The physical properties such as viscosities, densities and diffusivities are defined using Heaviside function, $H_\varepsilon(x)$ similar to Yang and Mao [20] as shown in the following

$$H_\varepsilon(x,y) = \begin{cases} 1, & \text{when x} \leq \mathbf{X} \\ 0, & \text{when x} > \mathbf{X} \end{cases} \tag{19}$$

Where $\mathbf{X}$ is the position of the interface. Using above function, the equation for any physical property, ϕ of the k^{th} phase, can be written as

$$\phi = \phi_2 + (\phi_1 - \phi_2) H_\varepsilon(x,y) \tag{20}$$

However, in the case of partition coefficient(m), the gradients instead of values were scaled and thus the three terms in convection-diffusion equation 16 were written as:

$$\frac{\partial \hat{C}}{\partial t} = \frac{\partial \hat{C}_{12}}{\partial\left(\frac{1}{\sqrt{m}}t\right)} + \left(\frac{\partial \hat{C}_{11}}{\partial(\sqrt{m}t)} - \frac{\partial \hat{C}_{12}}{\partial\left(\frac{1}{\sqrt{m}}t\right)}\right) H_\varepsilon(x,y) \tag{21}$$

$$\mathbf{u}\cdot\nabla\hat{C} = \sqrt{m}u_2\cdot\nabla\hat{C} + \left(\frac{1}{\sqrt{m}}u_1\cdot\nabla\hat{C} - \sqrt{m}u_2\cdot\nabla\hat{C}\right) H_\varepsilon(x,y) \tag{22}$$

$$\begin{aligned}\nabla\cdot(\hat{D}\nabla\hat{C}) = {} & \sqrt{m}\nabla\cdot(D_{12}\nabla\hat{C}) \\ & + \left(\frac{1}{\sqrt{m}}\nabla\cdot(D_{11}\nabla\hat{C}) - \sqrt{m}\nabla\cdot(D_{12}\nabla\hat{C})\right) H_\varepsilon(x,y)\end{aligned} \tag{23}$$

As we know, in most of the cases, more than one species participates in the chemical reaction. So each additional species requires an appropriate convection-diffusion equation. In the present work, we have solved convection-diffusion-reaction equations using straightforward operator splitting strategy described in [10] i.e. first of all scaler quantities are transported without taking the source/sinks into account. The convection-diffusion equations of each species are processed in parallel and the updated concentrations were used as initial data for a system of reaction ODEs, which describes the accumulation and consumption of a particular species. Thus, for the reaction calculation the generalised equation 17 was splitted as:

$$\frac{\partial \hat{C}_{ik}}{\partial t} + \mathbf{u} \cdot \nabla \hat{C}_{ik} - \nabla \cdot (\hat{D}_{ik} \nabla \hat{C}_{ik}) = 0 \tag{24}$$

$$\frac{\partial \hat{C}_{ik}}{\partial t} = r_{ik} \tag{25}$$

It is important to note that the operator splitting strategy was applied locally in time, i.e. within each time step,$\triangle t_n = t_{n+1}$ - t_n. The equidistant time stepping was used for all simulations and was refined for the mass transfer and reaction calculations. Since the multigrid solver was used for the simulations, the time step has to be refined with the level of mesh refinement. In most of the simulations a time step of 1×10^{-3}s was used for velocity, pressure and mass transfer with and without reaction calculations upto a mesh size of 0.03 $\times$ slug diameter. However, with increased level of refinement, the time step for velocity and was not reduced below 1×10^{-4}s while it was reduced by a factor of 2 with each level of refinement for mass transfer calculations. In order to maintain the positivity of the species concentration a conventional flux correction technique, upwinding, was applied.

The simulations with various parameters were carried out on a Sun-Fire-880 computer system with a 900 MHz Sparcv9 processor. The simulation time was noted for each operating condition and it was observed that the first part of simulations, hydrodynamic simulations took a very short time of several minutes, the mass transfer simulations took few hours while the reactions simulations took several hours to get the solutions for a mesh independent level of refinement.

3 Results and discussion

3.1 Fluid flow

Several simulations with different geometries and operating conditions with various viscosity combinations were carried out to study the flow behaviour within the slugs. The typical computational domain and its mesh, with more refinement near the interface and periodically connected interface in order to capture the sharp gradients of the variables, especially species concentration, is shown in the Figure 2. The negative velocity was defined at the wall while the slug was kept stationary. Figure 3 shows a simulated snapshot of the

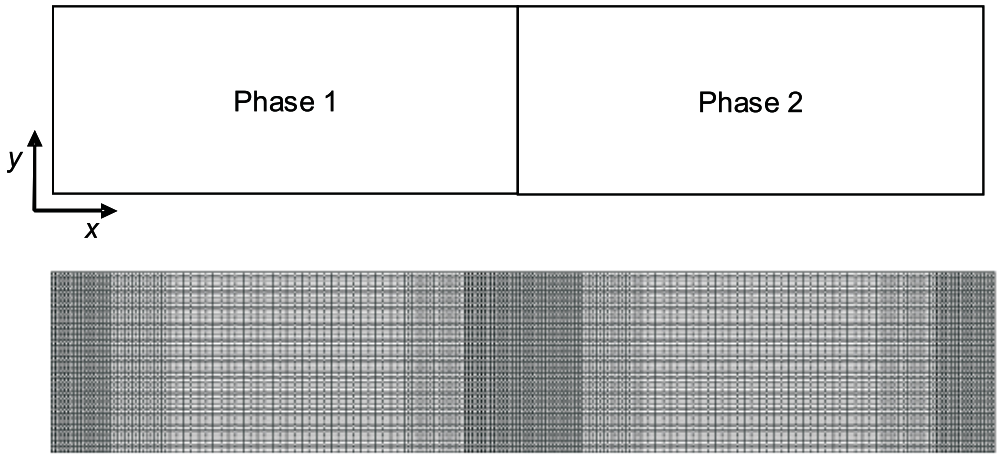

Fig. 2. Computational domain and mesh, showing the more refined mesh in the vicinity of the interface and periodically connected interface

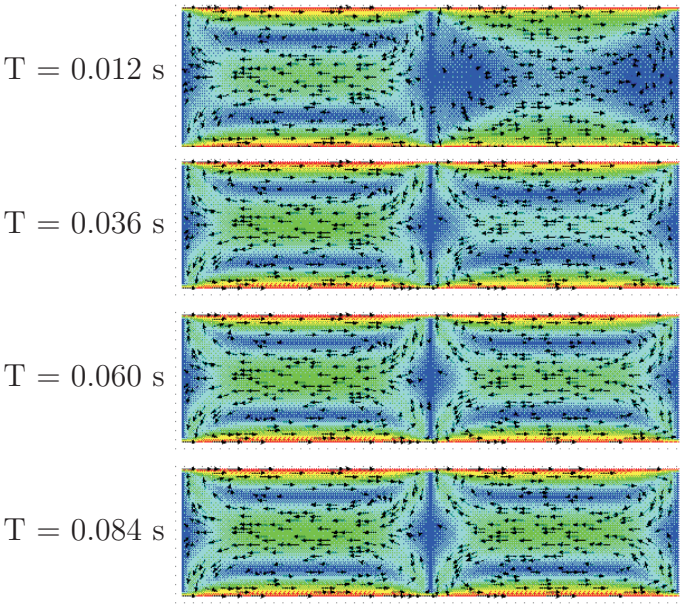

Fig. 3. Flow development for different viscosities in a slug unit (Left slug kinematic viscosity = $0.3\times10^{-5}m^2/s$ and right slug kinematic viscosity = $0.3\times10^{-3}m^2/s$)

velocity profiles in both slugs for a slug with 2 mm length and 0.5 mm width.

It was observed that a high viscosity fluid takes more time to achieve steady-state compared to a low viscosity fluid. Slug 1 contains the fluid with a

kinematic viscosity of 0.3×10^{-5} m^2/s while slug 2 contains a fluid with 0.3×10^{-3} m^2/s. The velocity vector plot shows that slug 1 has achieved steady state within a short time of around 0.012s while slug 2 has taken 0.084 s at an average slug flow velocity of 0.01 m/s, which is typical capillary flow velocity. However, it is still not fully developed pressure field and pressure takes a long time to achieve steady-state as compared to velocity.

The steady-state velocity profile achieved shows a maximum velocity at the centre line and minimum velocity at the wall, with a fully developed parabolic (Poiseuille) profile. Two flow patterns were observed within each slug: a recirculation zone at the centre and in the interface proximity and two stagnant zones in between them. When the slug moves through the capillary, due to the shear between slug axis and capillary wall, the liquid in the centre moves to the front end of the slug, where it contacts the front interface and returns back along the wall of the capillary while at the back end, liquid moves from the wall to the centre of slug and thus circulation takes place. The average flow velocity has strong effects on the bidirectional profile or recirculation. With increase in the average flow velocity, internal circulation increases, and thereby enhances convective mass transfer. The effect of average flow velocity and slug size is discussed in detail in ([7],[13]) and shows a strong effect of slug geometry on recirculation patterns. The present work was restricted to the flat interfaces, while the effect of true curved interface can be modelled using free surface modelling, which will be the subject of future.

3.2 Mass transfer

For mass transfer, the equations were solved in transient manner as discussed in the above section. Many simulations were carried out with different combinations of parameters to study the mass transfer in detail. As a test case, a slug unit with each slug has length of 1 mm with mass transfer of a species from phase 1 to 2 is presented here. The properties given in the Table 1 are defined corresponding to the extraction of succinic acid from its aqueous solution with n-butanol. The species is transported due to diffusion across the interface and keeps on recirculating due to internal circulations that arise. These circulations keep on renewing the interfacial concentration at the interface and increases the concentration gradient between two slugs which enhances the rate of mass transfer.

Table 1
Data used for mass transfer simulations

Flow ratio (aqueous/organic)	1	-
Slug length	1	mm
Slug diameter(D)	0.5	mm
Slug flow velocity	1.41	mm/s
Density ratio (Phase 1/phase 2)	1.25	-
Viscosity ratio (Phase 1/phase 2)	0.27	-
Initial concentration of species in phase 1	10	kg/m^3
Initial concentration of species in phase 1	0	kg/m^3
Partition coefficient (m)	1.17	-
Smallest cell size	0.008D	mm
Smallest time step for velocity and pressure	1 x 10^{-4}	s
Smallest time step for mass transfer	1 x 10^{-5}	s

Before calculating the actual variables/parameters, several simulations were carried out to make the solution grid independent. The domain was meshed in different ways: uniform mesh and mesh refined in the vicinity of the interface. In the first case, more computational power was required to solve a problem, while the total number of cells could be reduced in the later case but it was necessary to optimise the mesh. For a given number of cells in a domain, the mesh refined in the vicinity of the interfaces performs better and a significant difference in the concentration profiles was observed. So it was decided to use the refined mesh in the vicinity of the interface for further simulations.

The total concentration of the species in a particular region at each time step was determined by averaging it over the total number of nodes in that region. The volumetric mass transfer coefficient, k_La, of a species diffusing from phase 1 to phase 2 over the time period, t, from 0 to T is calculated as follows:

$$k_La = \frac{1}{T} ln \frac{(C_{2,sat} - C_{2,t=0})}{(C_{2,sat} - C_{2,t=T})} \tag{26}$$

where $C_{2,sat}$ is the saturation concentration of the species in phase 2. The well-defined specific interface area, a, in a microreactor enables the precise

calculation of overall mass transfer coefficient, k_L by the following equation.

$$k_L = \frac{1}{aT} ln \frac{(C_{2,sat} - C_{2,t=0})}{(C_{2,sat} - C_{2,t=T})} \tag{27}$$

The total simulation time, which is the residence time of the species in the reactor can be calculated from the length of the capillary, L, and slug flow velocity, V_s.

$$T = \frac{L}{V_s} \tag{28}$$

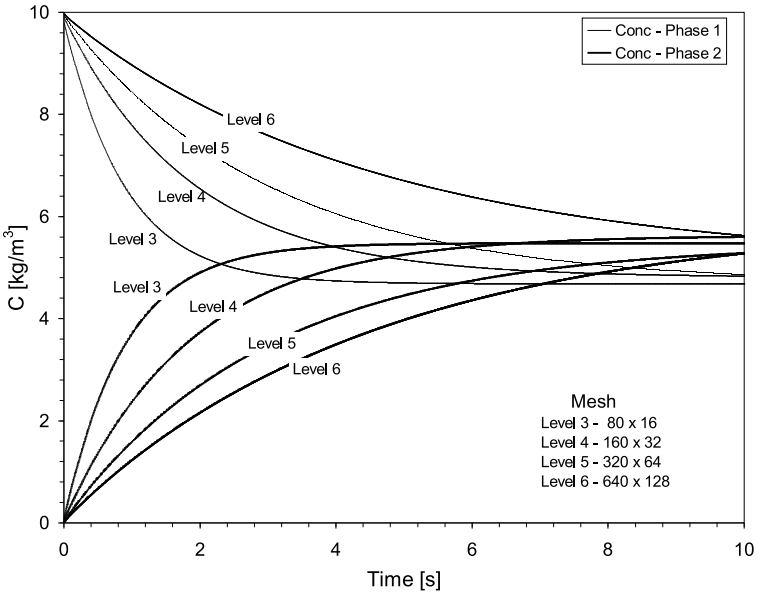

Fig. 4. Concentration profiles for different level of refinement

Figures 4-5 show the concentration profiles and mass transfer coefficients with respect to time for different meshes. With increase in the time, the concentration of species in phase 1 decreases while the concentration in the phase 2 increases. The saturation point, where the concentration curve of phase 2 remains constant, exhibit a slight difference for different levels of refinement while the concentration profiles before saturation shows a significant difference. The same effect of the mesh size was observed for mass transfer coefficients.

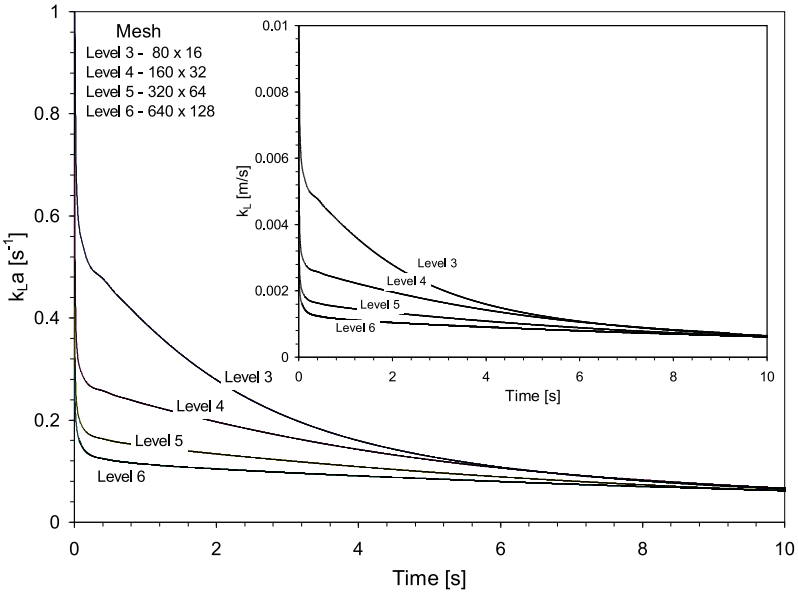

Fig. 5. Volumetric mass transfer coefficient, k_La and mass transfer coefficient, k_L for different level of refinement

3.3 Chemical reaction

For the chemical reaction, a titration reaction system was chosen and the range of operating parameters was taken from the experimental results of Harries *et. al.* [5]. This reaction for liquid-liquid slug flow system has been studied by in a glass microchannel by experimentation and CFD simulations. In this reaction system the acetic acid present in the kerosene phase is extracted with water where it reacts with the base, KOH/NaOH, producing salt and water. The representation of the system is shown in Figure 6. The partition behaviour studied experimentally have shown strong partition of acetic acid in favour of the aqueous phase, since the partition coefficient is 85. The reaction takes place in the aqueous phase and is extremely rapid as given by the following equations:

$$KOH + CH_3COOH \rightarrow CH_3COO^-K^+ + H_2O \tag{29}$$

$$NaOH + CH_3COOH \rightarrow CH_3COO^-Na^+ + H_2O \tag{30}$$

The same system of mass transfer equations need to be extended with the additional source or sink term to represent the reaction. The reaction is second order and only takes place in the aqueous phase. The convection-diffusion-reaction equations for the species in the water phase are given

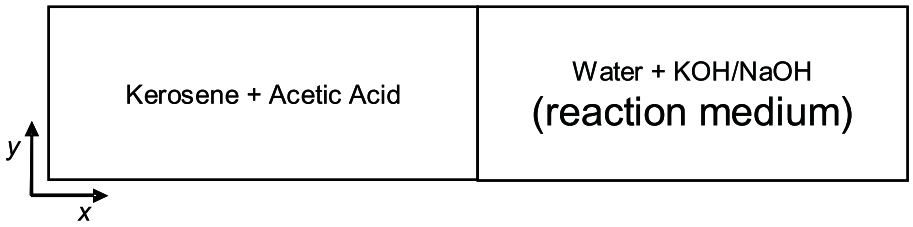

Fig. 6. Representation of species for reaction

by

$$\frac{\partial C_{12}}{\partial t} + u_2 \cdot \nabla C_{12} = D_{12}\Delta C_{12} - KC_{12}C_{22} \tag{31}$$

$$\frac{\partial C_{22}}{\partial t} + u_2 \cdot \nabla C_{22} = D_{22}\Delta C_{22} - KC_{12}C_{22} \tag{32}$$

$$\frac{\partial C_{32}}{\partial t} + u_2 \cdot \nabla C_{32} = D_{32}\Delta C_{32} + KC_{12}C_{22} \tag{33}$$

$$\frac{\partial C_{42}}{\partial t} + u_2 \cdot \nabla C_{42} = D_{42}\Delta C_{42} + KC_{12}C_{22} \tag{34}$$

where C_{12}, C_{22}, C_{32} and C_{42} are the concentrations of CH_3COOH, KOH or NaOH, $CH_3COO^-K^+$ or $CH_3COO^-Na^+$ and H_2O in phase 2 (water), respectively. However, as the acetic acid is present in both phases, it is governed by the equations 14-15. Since the second reactant (species 2) and products are present in the aqueous phase only, their exclusion from the kerosene phase was restricted by setting diffusion coefficient equal to zero as well as by setting the velocity, u_1 equal to zero in the kerosene slug region. Therefore, species 2, 3 and 4 will not diffuse through the interface and will remain in aqueous phase alone.

The concentrations which were obtained in the solution of convection-diffusion equation were used as initial data for the solution of ODEs, which are usually solved by explicit methods. However, this reaction is extremely rapid with the rate constant of $1.35\times10^{11}\ Lmol^{-1}s^{-1}$ and therefore, for a given time step it produces very high non-realistic value of the updated concentration of the products C_{32} and C_{42}. This problem could be solved using very small time step, but this is not feasible, because the computational time will increase significantly. Therefore an implicit treatment was employed and the solution of ODE from time t_n to t_{n+1} is updated for reactants and products in the following manner:

$$\begin{aligned} Reactants : \hat{C}_{i2}^{n+1} &= -K\hat{C}_{12}^{n+1}\hat{C}_{22}^{n+1} \triangle t + \hat{C}_{i2}^{n} \\ Products : \hat{C}_{i2}^{n+1} &= K\hat{C}_{12}^{n+1}\hat{C}_{12}^{n+1} \triangle t + \hat{C}_{i2}^{n} \end{aligned} \tag{35}$$

where, C_{i2} is the i^{th} species concentration in water phase and K is the rate constant of the reaction. This equation was solved and corresponding changes in the reactant and products were obtained for each node. Since the interface is represented by a straight line, it reduces the interfacial surface area for mass transfer and therefore an adjustment factor was applied to compensate the titration time i.e. the time required to complete disappearance of the base. The average values of the concentrations over the domains were obtained as for mass transfer and titration time at an average concentration of reactant NaOH/KOH, C_{22} equals 5% was used to compensate for the titration time difference due to flat interface [5].

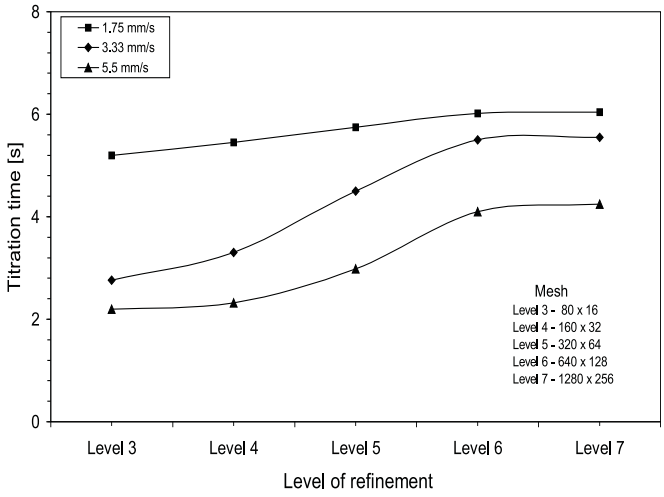

Fig. 7. Variation of titration time with respect to levels of refinement

As mentioned in the earlier sections, the simulations were carried out in a transient manner for the operating conditions shown in Table 2. The steady-state velocity profiles were established and then species transport calculations were done. Initially, the simulations were carried out in order to confirm the solution grid independence by doing simulations for various refinement levels. Figure 7 shows how the titration time was behaved with respect to the levels of refinement. In this case, the simulations were started at a relatively course mesh and were refined until the titration time difference between two consecutive levels becomes negligible. For this geometry, the course mesh was of size 0.25 $\times$ slug diameter and the mesh independent solution was obtained for level 6, which is equal to 0.008 $\times$ slug diameter.

The typical plot of concentration profiles of two reactants, CH_3COOH and

Table 2
Data used for chemical reaction simulation

Flow ratio (aqueous/organic)	1	-
Slug length range	1.5-3.8 1	mm
Slug diameter	0.38	mm
Slug flow velocity range	0.6-16.6	mm/s
Density ratio (kerosene/water)	0.8	-
Viscosity ratio (kerosene/water)	1.82	-
Initial concentration of CH_3COOH in kerosene	0.5	mol/lit
Initial concentration of CH_3COOH in water	0	mol/lit
Initial concentration of NaOH in water	0.25	mol/lit
Initial concentration of CH_3COONa in water	0	-
Partition coefficient for CH_3COOH (m)	85	-
Smallest cell size	0.008D	mm
Smallest time step for velocity and pressure	1×10^{-4}	s
Time step for mass transfer and chemical reaction	1×10^{-5}	s

$NaOH$ and a product, CH_3COONa in the aqueous phase for a slug with length 1.7 mm and flow velocity of 5.5 mm/s is shown in Figure 8. It shows that the concentration of CH_3COOH is very low in the aqueous phase which means that as it diffuses through the interface it reacts with the NaOH. Therefore the concentration of NaOH is decreases with time while the concentration of the product increases. When the entire NaOH in the water slug is consumed at time 4.15 sec, the amount of CH_3COOH increases in the water slug due to its excess stichometric proportion. The same behaviour revealed from the simulation snapshots of concentration profiles of different species in both phases for a slug with length of 1.9 mm and flow velocity of 3.33 mm/s with time shown in Figure 9.

The simulated results are compared with experimental and numerical results (from the correlations) of Harries *et. al.* [5]. The results show very good agreement with both sets of values as shown in Figure 10. At high and intermediate flow velocities, it shows very good agreement while at low velocity it slightly overpredicts the results. The discrepancy in the experimental and simulation results (of Harries et. al. and present model) is due

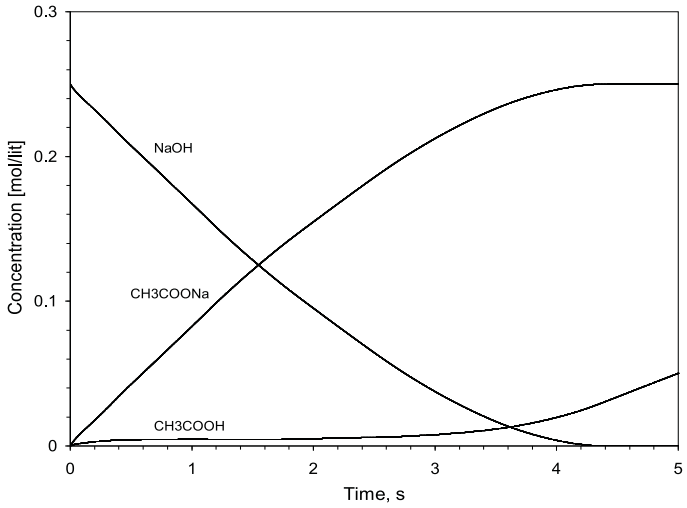

Fig. 8. A typical plot of average concentrations of three species in water slug (slug length = 1.7 mm, slug flow velocity = 5.5 mm/s)

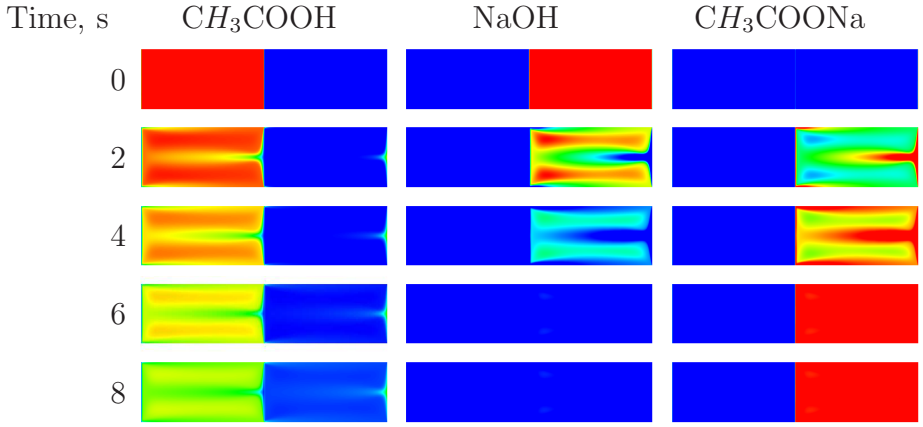

Fig. 9. Snapshots of concentration profiles of CH_3COOH, NaOH and CH_3COONa(slug length = 1.9 mm, slug flow velocity = 3.33 mm/s)

to several possible reasons. One of them could be that the assumption of flat interface which has strong effect on the velocity profile. The other may be the presence of a wall film in the microreactor used by Harries *et al.* [5]. In our laboratory experiments with PTFE capillary tube, it was demonstrated that, due to the superior wetting properties of the organic liquid phase on PTFE, an organic wall film is present.

The model showed improvement in comparison with the literature results for titration time as well the computational time requirement. In future

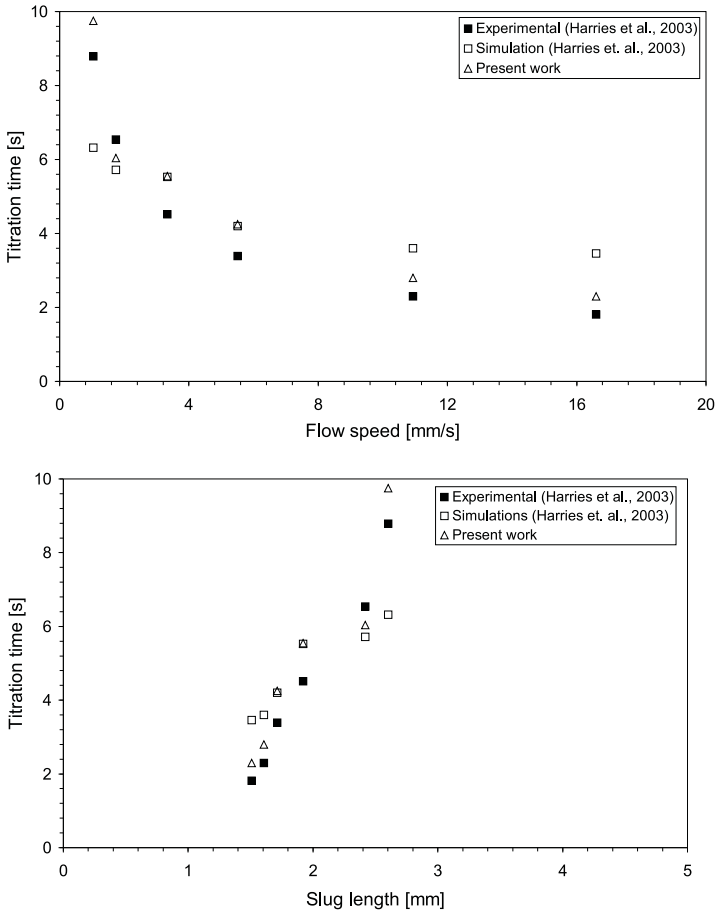

Fig. 10. Plot of titration time vs flow speed and titration time vs slug length

studies, the model will be extended in order to incorporate free surface hydrodynamics. For curved interface, secondary circulatory flow generation takes place in the vicinity of the interface, which has significant effect on the hydrodynamics. In this case, a free surface simulation without mass transfer will first be carried out. The steady-state velocity profile obtained will then be incorporated into the present model. As mentioned above, the phenomenon of the organic wall film will be included and the results will be compared with our experimental results.

4 Conclusion

A CFD model was developed to simulate the mass transfer with and without chemical reaction for the liquid-liquid slug flow capillary microreactor. Several simulations were carried out to elucidate the fluid flow and mass transfer behaviour. Finally, the model was validated with a published example of titration reaction and it was observed that the experimental and simulated results presented in the literature are in very good agreement with it. This model can be applied for any liquid-liquid system with fixed interfacial location. In the future work, the model will coupled with free surface models, in order to capture the complex hydrodynamics in the vicinity of the interface.

Acknowledgements

The authors acknowledge the contributions of Dr. Jaroslav Hron, Dr. Abderrahim Ouazzi and Dr. Otto Mierka for useful discussions and suggestions about this topic.

References

[1] Bothe Dieter, Koebe Mario, Wielage Kerstin and Warnecke Hans-Joachim, VOF simulations of mass transfer from single bubbles and bubble chains rising in the aqueous solutions, Proceedings of FEDSM03: 4th ASME-JSME joint fluids engineering conference, Honolulu, Hawaii, USA, July 6-11, 2003.

[2] Burns, J. R. and Ramshaw, C., The intensification of rapid reactions in multiphase systems using slug flow in capillaries, Lab on a Chip, 1, 10-15, 2001.

[3] Dummann Gerrit, Quittmann Ulrich, Groschel Lother, Agar David, W., Worz Otto and Morgenschweis Konard, The capillary microreactor: a new reactor concept for the intensification of heat and mass transfer in liquid-liquid reactions, Catalysis Today, 79-80, 433-439, 2003.

[4] Hardt, S and Schonfeld, F., Simulation of hydrodynamics in multiphase microreactors, Fifth world congress on computational mechanics, Vienna, Austriya, July 7-12, 2002.

[5] Harries, N., Burns, J. R., Barrow, D. A. and Ramshaw, C. A numerical model for segmented flow in a microreactor, International Journal of Heat and Mass Transfer, 46, 3313-3322, 2003.

[6] Hirt, C.W., and B.D. Nichols, Volume of fluid (VOF) method for the dynamics of free boundaries," Journal of Computational Physics, 39, 201-225, 1981.

[7] Kashid, M. N., Gerlach, I., Goetz, S., Franzke, J., Acker, J. F., Platte, F., Agar, D. W. and Turek, S., Internal circulation within the liquid slugs of liquid-liquid slug flow capillary microreactor, Industrial and Engineering Chemistry Research, 44(14), 5003-5010, 2005.

[8] Kashid, M. N., Platte, F., Agar, D. W. and Turek, S., Computational modelling of slug flow in a capillary microreactor, Journal of computational and applied mathematics, Accepted for publication.

[9] Kreutzer Michiel, Hydrodynamics of Taylor flows in capillaries and monolith reactors, Ph.D Thesis, Delft University Press, The Netherlands, 2003.

[10] Kuzmin, D. and Turek, S., Finite element descretisation tools for gas-liquid flows. In: M. Sommerfeld (ed.), Bubbly Flows: Analysis, Modelling and Calculation, Springer, 2004, 191-201.

[11] Ming Hsing, I., Srinivasan Ravi, Harold Michael, P., Jensen Klavs, F. and Schmidt Martin, A., Simulation of micromachined chemical reactors for heterogenous partial oxidation reactions, Chemical Engineering Science, 55, 3-13, 2000.

[12] Taha, T. and Cui, Z. F., Hydrodynamics of slug flow inside capillaries, Chemical Engineering Science, 59, 1181-1190, 2004.

[13] Tanthapanichakoon, W., Aoki, N., Matsuyama, K., and Mae, K., Design of mixing in microfluidic liquid slugs based on a new dimensionless number for precise reaction and mixing operations, Chemical Engineering Science, 61, 4220-4232, 2006.

[14] Thulasidas, T. C., Abraham, M. A. and Cerro, R. L., Flow pattern in liquid slugs during bubble train flow inside capillaries, Chemical Engineering Science, 52(17), 2947-2962, 1997.

[15] Turek, S., Efficient solvers for incompressible flow problems: an algorithmic approach, Springer-Verlag, Heidelberg, 1999.

[16] Ouazzi, A., Finite element simulation of non-linear fluids with application to granular material and powder, PhD Thesis, University of Dortmund, Germany, 2006.

[17] Piarah, W. H., Paschedag, A. and Kraume, M., Numerical simulation of mass transfer between a single drop and ambient flow, AICHE Journal, 47(7), 2001.

[18] van Baten, J. M. and Krishna, R., CFD simulations of mass transfer from Taylor bubbles rising in circular capillaries, Chemical Engineering Science, 59, 2535-2545, 2004.

[19] van Sint Annaland, M., Dijkhuizen, W., Deen, N. G. and Kuipers, J. A. M., Numical simulation of behaviour of gas bubbles using a 3D front tracking method, AIChE Journal, 52(1), 99-110, 2006.

[20] Yang Chao and Mao Zai-sha, Numerical simulation of interphase mass transfer with the levelset approach, Chemical Engineering Science, 60, 2643-2660, 2005.